



Mantle flow influence on subduction evolution

Maria V. Chertova^a, Wim Spakman^{a,b,*}, Bernhard Steinberger^{c,b}

^a Department of Earth Sciences, Utrecht University, The Netherlands

^b Centre of Earth Evolution and Dynamics (CEED), University of Oslo, Norway

^c GFZ German Research Centre for Geosciences, Germany

ARTICLE INFO

Article history:

Received 15 June 2017

Received in revised form 19 January 2018

Accepted 25 February 2018

Available online 12 March 2018

Editor: B. Buffett

Keywords:

mantle flow

subduction

Mediterranean

3-D numerical modeling

ABSTRACT

The impact of remotely forced mantle flow on regional subduction evolution is largely unexplored. Here we investigate this by means of 3D thermo-mechanical numerical modeling using a regional modeling domain. We start with simplified models consisting of a 600 km (or 1400 km) wide subducting plate surrounded by other plates. Mantle inflow of ~ 3 cm/yr is prescribed during 25 Myr of slab evolution on a subset of the domain boundaries while the other side boundaries are open. Our experiments show that the influence of imposed mantle flow on subduction evolution is the least for trench-perpendicular mantle inflow from either the back or front of the slab leading to 10–50 km changes in slab morphology and trench position while no strong slab dip changes were observed, as compared to a reference model with no imposed mantle inflow. In experiments with trench-oblique mantle inflow we notice larger effects of slab bending and slab translation of the order of 100–200 km. Lastly, we investigate how subduction in the western Mediterranean region is influenced by remotely excited mantle flow that is computed by back-advection of a temperature and density model scaled from a global seismic tomography model. After 35 Myr of subduction evolution we find 10–50 km changes in slab position and slab morphology and a slight change in overall slab tilt. Our study shows that remotely forced mantle flow leads to secondary effects on slab evolution as compared to slab buoyancy and plate motion. Still these secondary effects occur on scales, 10–50 km, typical for the large-scale deformation of the overlying crust and thus may still be of large importance for understanding geological evolution.

© 2018 Elsevier B.V. All rights reserved.

1. Introduction

The dynamical and morphological evolution of subducting slabs has for decades been widely investigated by means of 2D and eventually 3D numerical and laboratory modeling. 3D modeling brought focus on the feedback between slab-induced mantle flow and slab evolution with particular attention for the trench-parallel flow and toroidal flow occurring around the edges of a retreating slab (e.g. Kincaid and Griffiths, 2003; Funiciello et al., 2003, 2004, 2006; Schellart, 2004; Piromallo et al., 2006; Stegman et al., 2006; Schellart et al., 2007; Stegman et al., 2010; Butterworth et al., 2012; Capitanio and Faccenda, 2012; Jadamec and Billen, 2012; Schellart and Moresi, 2013; MacDougall et al., 2014; Crameri and Tackley, 2014; Sternai et al., 2014). These 3D modeling studies have demonstrated the importance of mantle flow that is induced by slab motion, but how remotely forced mantle flow affects slab evolution remains unexplored. By remotely forced, or external, mantle flow we mean flow that is caused by plate motions and subduc-

tion elsewhere or is excited by deeper mantle processes such as rising plumes or sinking of detached slab. Slab-induced flow resulting from e.g. slab rollback can be perceived as superposed on, or interacting with this background flow. Until now only a few papers (Hager et al., 1983; Olbertz et al., 1997; Boutelier and Cruden, 2008; Winder and Peacock, 2001; Rodríguez-González et al., 2014; Ficini et al., 2017) paid attention to the possible influence of remotely forced mantle flow on subduction evolution. These studies demonstrate a strong influence on slab geometry evolution but due to the 2D nature of the modeling, not allowing for toroidal mantle flow, such inferences are restricted to geodynamic settings in which poloidal flow strongly dominates.

Here we investigate the impact of remotely forced mantle flow on subduction evolution with 3D thermo-mechanical numerical modeling using a regional modeling domain by imposing mantle inflow on a subset of the side boundaries. As this topic is unexplored in 3-D our primary purpose is to browse through the model space searching for first-order effects. We monitor the evolution of slab morphology under different external mantle flow conditions both for generic subduction models and for a simulation of natural subduction in the western Mediterranean. For

* Corresponding author.

E-mail address: W.Spakman@uu.nl (W. Spakman).

the generic simulations, we use simplified models of subduction evolution comprised of rectangular plates and a straight trench with initial trench-perpendicular plate convergence. This is done to make a link with this often-used model setup in 3-D subduction modeling. We include in our experiments the overriding plate and plates adjacent to the subducting plate, similar to recently used model setups (e.g. Yamato et al., 2009; Capitanio et al., 2010; Butterworth et al., 2012; Meyer and Schellart, 2013; Boutelier and Cruden, 2013; Guillaume et al., 2013; Moresi et al., 2014). We combine side boundaries with prescribed mantle flow with side boundaries that are open (Chertova et al., 2012, 2014a, 2014b) for conservation of mass. Because free-slip boundary conditions are most often used in 3D subduction modeling using a regional model domain, we briefly address the magnitude of the difference between using either boundary condition in the experiments we conduct here. Lastly, we investigate the influence of remotely forced mantle flow in a simulation of the Rif–Gibraltar–Betic subduction evolution since ~35 Ma in the western Mediterranean region. This builds on our earlier work for this subduction system (Chertova et al., 2014a, 2014b) in which we used open side boundaries. In these experiments, we impose time-dependent boundary conditions of mantle flow determined from back-advection of the present-day temperature and density structure of the mantle derived from a tomographic model. These experiments also serve to test the robustness of the earlier modeled subduction evolution (Chertova et al., 2014a, 2014b) with respect to the viscous forcing exerted on the slab by remotely forced mantle flow.

2. Methodology

We carry out our 3-D numerical experiments using the finite element package SEPRAN (Segal and Praagman, 2005). As described in Chertova et al. (2014a, 2014b), we solve the equations of mass, momentum and energy conservation and the transport equation for advection of non-diffusive material properties using the extended Boussinesq approximation including two major phase transitions at 410 km and at 660 km in the unperturbed mantle. Experiments are performed in a Cartesian box with dimensions of length \times width \times height = 3000 km \times 2000 km \times 1000 km for the generic model setup and 1800 km \times 1300 km \times 1000 km for the simulation of western Mediterranean subduction.

2.1. Rheology and boundary conditions

Composite nonlinear rheology is used for all models and comprises diffusion creep, dislocation creep, and a viscosity maximum, $\eta_{\max}(2 \times 10^{23}$ or 5×10^{23} Pas). For the geometrically more complex western Mediterranean model setup also a stress limiter mechanism is used (Chertova et al., 2014a, 2014b). The effective composite viscosity is defined as $\frac{1}{\eta_{\text{eff}}} = \frac{1}{\eta_{\text{diff}}} + \frac{1}{\eta_{\text{disl}}} + \frac{1}{\eta_y}$, with

$$\eta_{\text{diff}} = \mu A_{\text{diff}}^{-1} (b/d)^{-m} \exp[(E_{\text{diff}} + PV_{\text{diff}})/RT] \quad (2.1)$$

$$\eta_{\text{disl}} = \mu A_{\text{disl}}^{-\frac{1}{n}} \dot{\epsilon}^{\frac{1-n}{n}} \exp[(E_{\text{disl}} + PV_{\text{disl}})/nRT] \quad (2.2)$$

$$\eta_y = \frac{\tau_{\max}}{2\dot{\epsilon}}, \quad (2.3)$$

where μ is the shear modulus, $A_{\text{diff}}, A_{\text{disl}}$ are diffusion and dislocation creep viscosity prefactors, b is Burgers vector, d is the grain size, $\dot{\epsilon}$ is the second invariant of the strain-rate tensor, m is the grain size exponent, $V_{\text{diff}}, V_{\text{disl}}$ and $E_{\text{diff}}, E_{\text{disl}}$ are activation volume and activation energy for diffusion and dislocation creep, respectively, P is the lithostatic pressure, T is temperature, τ_{\max} is the maximum yield stress value, i.e. stress limiter. Used parameters for the rheology and phase transitions are given in supplementary

Table 1. Lagrangian particles are used to define viscosity parameters. They are placed randomly over the whole modeling domain and free inflow/outflow of particles is allowed on side boundaries. The number of particles varies between 20 and 30 million during computations. We use free-slip conditions for the top boundary and no-slip for the bottom boundary. Different side boundary conditions are used: free-slip (closed, impermeable boundary), open boundaries as developed in Chertova et al. (2012), or prescribed mantle flow at a subset of the vertical sides, as detailed in the next section. For all boundaries we prescribe a stationary depth-dependent adiabatic temperature profile during simulations. The mesh element size varies from 6 km in the top 200 km to 20 km at the bottom of the model.

To allow decoupling of the subducting slab from the free-slip top surface and overriding plate we implement a 30 km weak crustal layer, as in Chertova et al. (2012, 2014a, 2014b), with a viscosity 2×10^{19} Pas in the generic models and 5×10^{19} Pas for the western Mediterranean subduction modeling. This weak top layer facilitates vertical decoupling of the slab during the development of subduction, which is driven by its slab buoyancy, and by the subducting plate motion that is imposed on the side-boundary, both simulating geodynamic forcing that also occurs naturally. Additional forcing comes from the mantle flow imposed on selected boundaries of the model of which the effects on subduction evolution are topic of our investigation here.

2.2. Initial model setup for generic models

The initial model setup is illustrated in Fig. 1A and comprises the subducting and overriding plates and two plates to either side. Table 1 lists the models we created with the various inflow boundary conditions. All 4 plates have the same initial thermal structure determined from the equation of a cooling semi-infinite half space for an oceanic lithosphere age of 80 My. The initial subduction angle is 45° and the slab extends to the depth of 300 km. Low viscosity deformation zones of $3 \cdot 10^{20}$ Pas and 70 km wide (pink in Fig. 1A) are used as a weak mechanical coupling of the plates (Fig. 1B). Fig. 1B shows their motion decoupling effect between subducting and side-plates in the initial model stage. Experiments are performed with a subducting plate width of 600 and 1400 km. These models include a viscosity increase in the mantle by a factor of ~ 10 to 10^{22} Pas at a depth of ~ 660 km. The upper viscosity limit is set to $5 \cdot 10^{23}$ Pas. The activation energy for dislocation creep and activation volume for diffusion creep for most models is set to 423 KJ mol $^{-1}$ and 3 cm 3 mol $^{-1}$ respectively. But, for models M600.O*, M600.SE, M600.SW and M600.O/E/S a slightly higher activation energy of 433 KJ mol $^{-1}$ is used for reasons explained later. An example of viscosity profiles away from the subducting slab is shown in supplementary Fig. 1. In all models, we prescribe the speed of the subducting plate of 1.5 cm/yr on the western side boundary, which ensures that the slab does not rollback too fast to this side boundary. Although this choice is practical, it is not unnatural because slab pull and an independent component of advance velocity of the subducting plate are natural drivers of many subduction zones (e.g. Heuret and Lallemand, 2005; Schellart, 2008).

For model comparison, we constructed two reference models of subduction evolution, M600.O and M1400.O, in which 4 open boundaries are used and thus no mantle inflow is imposed. In separate experiments uniform inflow of the mantle at a speed of 3 cm/yr is prescribed below the lithosphere on either the western (left), eastern (right) or southern (frontal) model boundary keeping other boundaries open (Table 1). Transitions between boundary conditions are taken up locally and smoothly by the modeled mantle flow. Lastly, we created experiments where the prescribed mantle flow of 3 cm/yr gradually changes direction from eastward

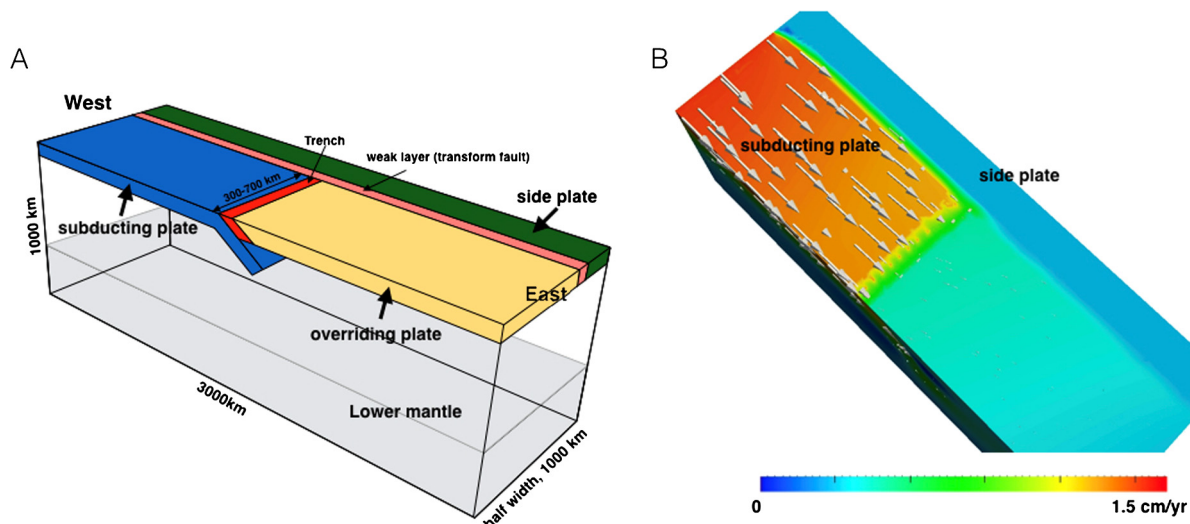


Fig. 1. A – Model setup for models with four plates shown up to the symmetry plane (front). The trench is located in 1400 km from the left boundary. B – Top view of the initial surface velocity field of the model for a subducting plate velocity of 1.5 cm/yr imposed on the top of the western model edge. Colors show the X-component (parallel to symmetry plane) of the velocity field and arrows-total magnitude and direction.

Table 1

List of numerical models. The number indicates the lateral width of the model slab. The letters after the “.” signify either open boundaries all around (“O”), or the model side where inflow occurs (“W”, “E”, “S”, “SW”, “SE”, for west, east, south, southwest, southeast, respectively). Western and eastern sides are indicated in Fig. 1 “W–S” denotes a model start starts with inflow from the west followed by inflow the south; “O/E/S” denotes a model that initially has open boundaries all around after which inflow occurs from the east gradually changing to inflow from the south; “FS” denotes a model with 2 free-slip boundaries; and “O*” is a model with 4 open boundaries with stronger rheology.

Model name	Mantle inflow conditions on the side boundary			
	Left (W)	Right (E)	Front (S)	Back (N)
M1400.O	Open	Open	Open	Open
M1400.W	3 cm/yr	Open	Open	Open
M1400.E	Open	3 cm/yr	Open	Open
M1400.S	Open	Open	3 cm/yr	Open
M1400.W–S	3 cm/yr	Open	3 cm/yr	Open
M600.O	Open	Open	Open	Open
M600.W	3 cm/yr	Open	Open	Open
M600.E	Open	3 cm/yr	Open	Open
M600.S	Open	Open	3 cm/yr	Open
M600.O*	Open	Open	Open	Open
M600.O/E/S	variable	Open	variable	Open
M600.SE	Open	3 cm/yr	3 cm/yr	Open
M600.SW	3 cm/yr	Open	3 cm/yr	Open
M600.FS	Open	Open	Free-slip	Free-slip
M600.FS–W	Free-slip	Open	Open	Open

to northward directed inflow during 10 My of subduction evolution and experiments where we prescribe mantle inflow from SW and SE directions, i.e. under an angle of 45° to the subducting slab. In addition, to briefly assess the influence of open versus closed boundaries we also used a free-slip condition on the northern and southern boundaries of which results are presented as supplementary Fig. 3.

2.3. Initial model setup for western Mediterranean models

The initial model setup for the western Mediterranean plate boundary region is defined at 35 Ma (Fig. 2) and follows that of Chertova et al. (2014a, 2014b). The paleogeography is derived from van Hinsbergen et al. (2014) and comprises the oceanic, or extremely stretched continental, basins that eventually lead to the Rif–Gibraltar–Betic (RGB) slab and to the eastern Algerian Kabyldes slab. We use absolute plate motion estimates (Dobrovine et al., 2012) averaged over the past ~ 35 Myr as kine-

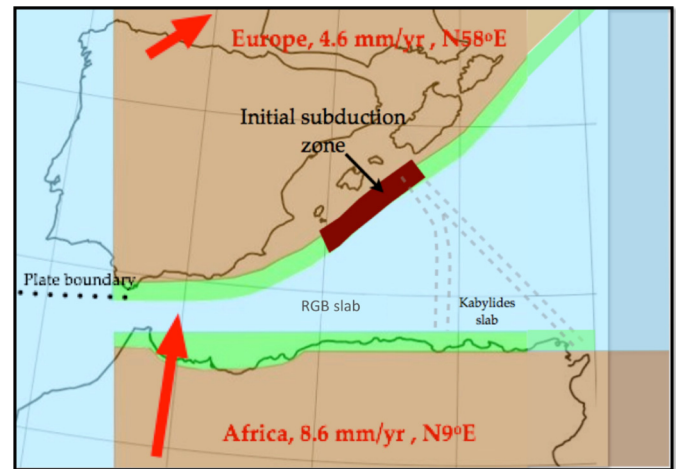


Fig. 2. The initial model for modeling western Mediterranean subduction ($2000 \times 1300 \times 1000$ km) comprises two domains of continental lithosphere (Europe and Africa; brown), a continuous domain of oceanic lithosphere (blue), two weak continental margins (green) and an initial subduction zone located to the SE from the Balears with a slab length of ~ 200 km (dark red). The oceanic domains labeled “RGB slab” and “Kabyldes slab” will be subducting in the model. Two double-dashed lines indicate the position of weak decoupling zones that simulate transform faults and separate the RGB (Alboran) and Kabyldes slab and the easternmost part of the oceanic domain. These weakness zones constitute 60 Ma oceanic lithosphere with a viscous strength of $2 \cdot 10^{20}$ Pas to facilitate decoupling between plates. Parameters used for the rheology were determined in Chertova et al. (2014a, 2014b). The initial temperature distribution within the oceanic lithosphere is determined from the equation of cooling semi-infinite half space for an age of 100 My and for continental lithosphere we use a constant temperature gradient of 10 K/km. For the mantle temperature, an adiabat with potential temperature of 1573 K is used instead of a constant temperature gradient as in Chertova et al. (2014a, 2014b). For other details we refer to that paper.

matic boundary conditions for the top 150 km at the southern boundary for Africa (8.6 mm/yr) and at the northern boundary for Iberia (4.6 mm/yr) with directions as illustrated in Fig. 2. For the remainder, the sidewalls are open boundaries and the bottom is no-slip.

3. Experiments with generic models

We start our modeling experiments with inflow normal to the trench from either the west or east and next parallel to the trench

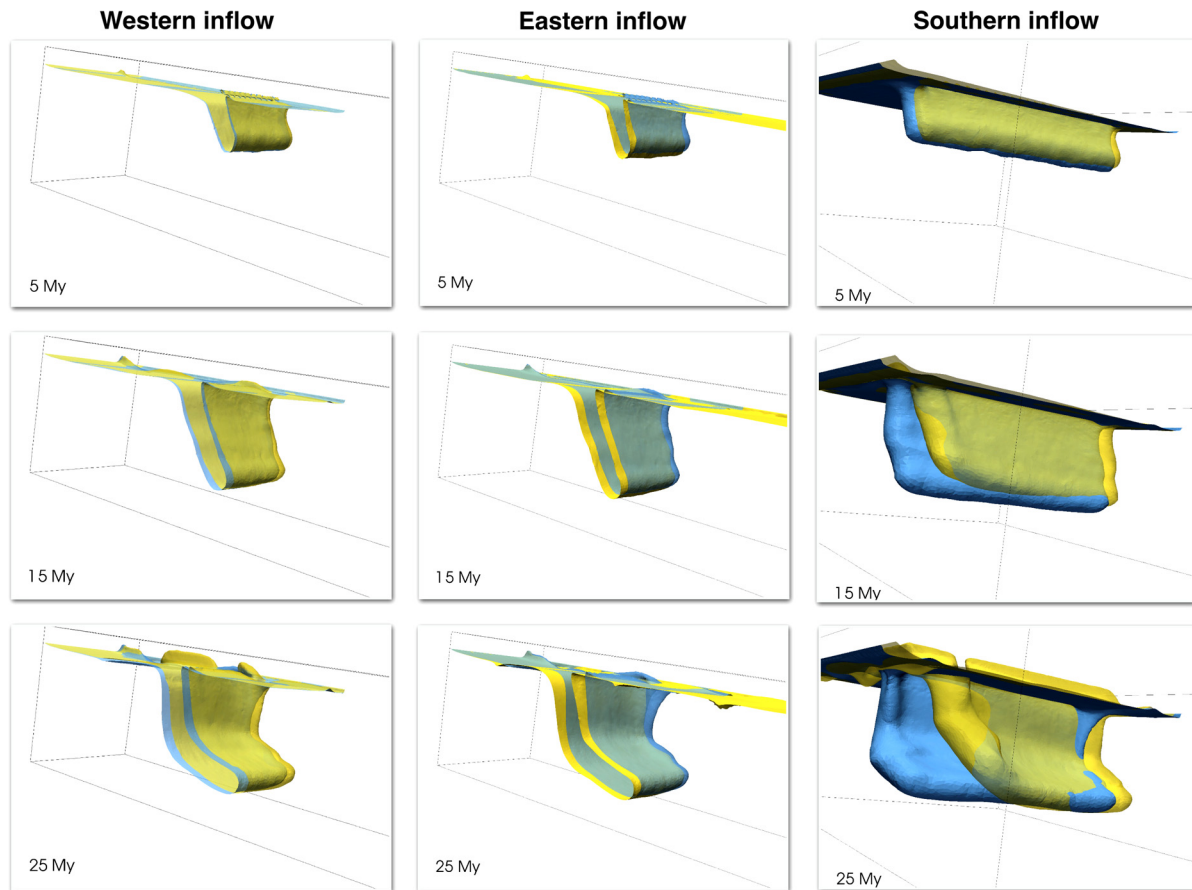


Fig. 3. Evolution of models M1400.W (western inflow), M1400.E (eastern inflow) and M1400.S (southern inflow); all in transparent yellow compared with the reference model M1400.O (transparent blue). Models with western and eastern inflow are given for the half-width of the modeling domain. The 1500 K isotherm defines the used contours.

from the south for both a 600 km wide and 1400 km wide slab. Following are various experiments with mantle inflow oblique to the trench. The results are compared to the reference models with open side boundary conditions and between models. Reference model M1400.O is briefly illustrated in supplementary material 1.

3.1. Influence of external mantle flow on the evolution of a wide subduction zone

Fig. 3 presents the evolution of three models with western (M1400.W), eastern (M1400.E) and southern (M1400.S) mantle inflow, all for a wide slab of 1400 km and compared to the reference model M1400.O (transparent blue).

In both M1400.W and M1400.E the slab position after 25 My of subduction evolution is displaced by 30–50 km with minor changes in overall slab shape for M1400.W. For model M1400.E this displacement occurs toward the west and a shallower subduction dip is observed in the top few hundred km, both resulting from the push exerted by inflow from the east, which effectively leads to a slight increase in slab rollback. In model M1400.W slab rollback is obstructed by the western inflow in the sub-slab mantle but this does not change the overall slab morphology as compared to the reference model.

For the model M1400.S with southern, trench parallel, mantle inflow we observe more dramatic changes toward the final slab morphology. Slab curvature in the horizontal plane increases with time and the slab is being transported to the north by the viscous coupling with the imposed mantle flow. The southern slab edge is elevated and thickened due to the impact of mantle flow. This slab deformation already starts during the initial subduction phase

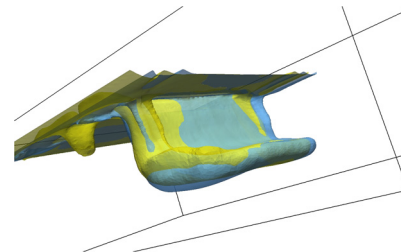


Fig. 4. Comparison at 30 Myr between model M1400.W, shown in transparent blue and shifted by 150 km to the north and model M1400.W-S shown in transparent yellow. The 1500 K isotherm defines the used contours.

when the slab is still short (~300 km). When a longer slab across the upper mantle is next subject to mantle inflow from the south, slab deformation is less pronounced as is demonstrated with the model M1400.W-S. After 20 Myr of subduction evolution under western mantle inflow, the direction of mantle inflow is changed to inflow from the south. This led to ~150 km of northward slab transport in 10 Myr. Fig. 4 shows the difference in slab morphology that accumulates between 20 Myr and 30 Myr in models M1400.W and M1400.W-S, where we have shifted model M1400.W to the north by 150 km to compare the slab shape in more detail. Uplift of ~40 km of the southern slab edge is observed and slab-edge thickening of the order of ~20 km compared to an original plate thickness 90–100 km. The rest of the slab stays relatively undeformed although still being transported 150 km to the north by the imposed mantle flow. This transport is accommodated by N–S shortening of the plate decoupling zone and of the northern side plate.

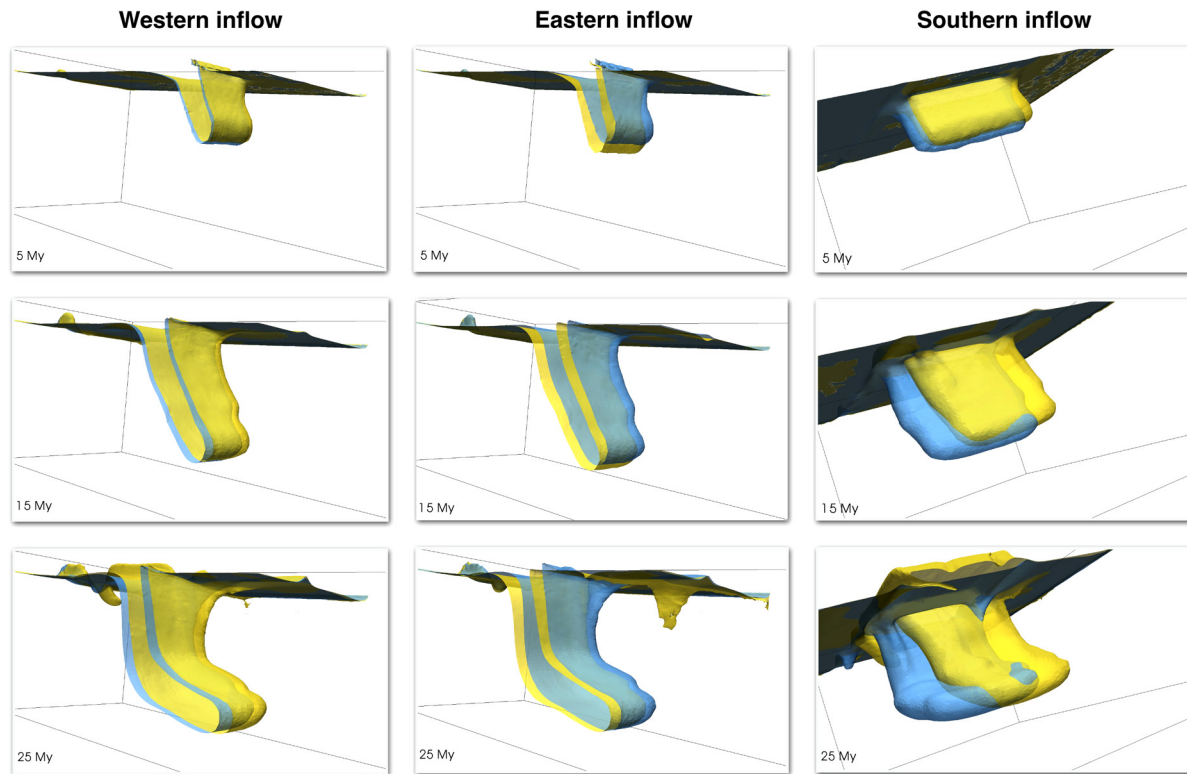


Fig. 5. Evolution of narrow-slab models M600.W (western inflow), M600.E (eastern inflow) and M600.S (southern inflow) compared to the reference model M600.O (blue transparent contour). Models with western and eastern inflow are given for the half-width of the modeling domain. The 1500 K isotherm defines the used contours.

3.2. Influence of external mantle flow on the evolution of a narrow subduction zone

Similar experiments were conducted with a 600 km wide subduction zone leading to models with western (M600.W), eastern (M600.E), and southern (M600.S) mantle inflow. In Fig. 5 results are compared to the reference model with open boundaries M600.O (transparent blue). With the same inflow conditions, model M600.O demonstrates slightly faster rollback that accumulates to ~60 km more westward displacement at 25 Myr than model M1400.O. For the 1400 km wide subduction zone, rollback is slower as it takes longer to move sub-slab mantle to both slab edges as also inferred previously (Schellart et al., 2007). For the models M600.W and M600.E we observe a difference of about 50–60 km in final trench position compared to the reference M600.O model, which is similar to what we observed for the 1400 km wide subduction zone. Another similarity between corresponding *.E and *.W models concerns the slab shape. For the model M600.S with trench-parallel inflow the mantle flow influence is not stronger than for the M1400.S model. The results show a smaller difference between M600.S and M600.O than between models M1400.S and M1400.O. The final slab in M600.S is less curved and less thickened and the tip of the slab is not uplifted as in the M1400.S model. However, the deeper part of the slab is transported more to the north than the top part as in the M1400.S model. The top 150 km of the side boundaries are fixed and deformation due to mantle flow is accommodated by the weak margins and by internal deformation of the side plates. In summary, the influence of prescribed western or eastern mantle inflow on the evolution of the narrow subduction zone is not stronger than for the wide subduction zone, except for a difference in rollback speed. We explain this by the fact that the total viscous coupling force exerted by mantle flow on the slab scales with the slab surface area.

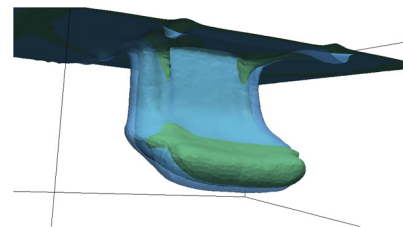


Fig. 6. Reference model M600.O (transparent blue) and model M600.O/E/S (green) after 20 My of the subduction evolution. View from southeast. The 1500 K isotherm defines the used contours.

3.3. Slab evolution under directionally variable and trench-oblique mantle inflow

In previous experiments the imposed mantle flow was either perpendicular or parallel to the slab, which is of course not necessarily mimicking natural conditions. To assess the influence of imposed trench-oblique mantle flow we devised three models. In model M600.O/E/S imposed flow gradually changes direction with time, while for models M600.SW and M600.SE the imposed flow is oriented at 45° to the subduction zone inflowing from the SW and from the SE, respectively.

Fig. 6 shows the difference between reference model M600.O and M600.O/E/S after 20 My of subduction evolution. During the first 10 My model M600.O/E/S has the same open boundary conditions as for the reference model. Next, we prescribe mantle inflow of 3 cm/yr that gradually changes from eastward inflow to southern inflow between 10 My and 20 My. Model M600.O/E/S exhibits several differences with the M600.O model. The slab in model M600.O/E/S bends, the southern edge gets thicker, and the lateral width of the shallow part of the slab (to the depth of 300 km) decreases by ~50 km. This leads to increased curvature of the slab and its central part lies ~20 km to the west of the reference model. The position of the slab tip is ~10 km shallower than

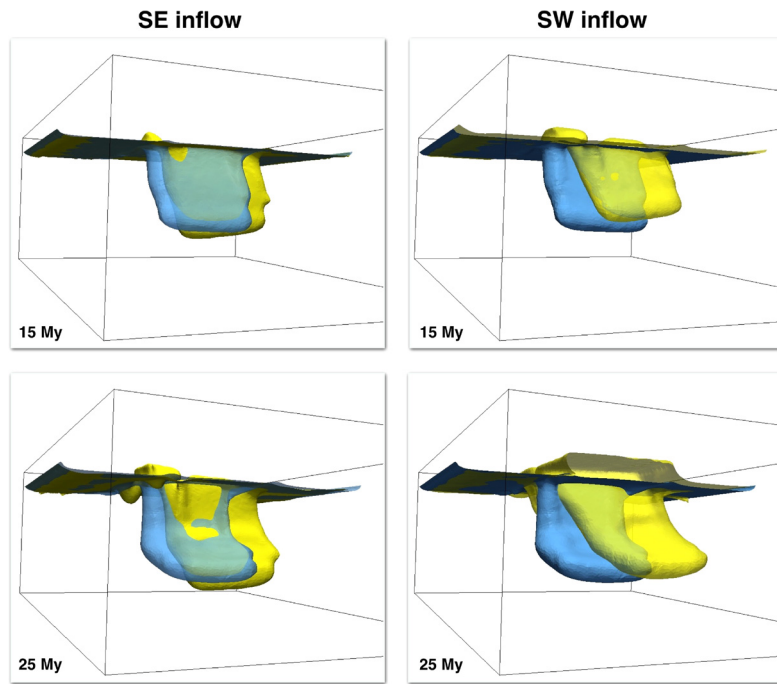


Fig. 7. Comparison of models M600.SE (SE inflow) and M600.SW (SW inflow) with reference model M600.O* (blue) at 15 Myr and 25 Myr of slab evolution. The 1500 K isotherm defines the used contours.

in the reference model. Overall these differences with the reference model are relatively small (10–50 km), compared to the scale of the subduction zone, but they do show sensitivity of the slab to oblique time-variable mantle flow leading to complex slab morphology accumulating in only 10 Myr.

In Fig. 7 we show snapshots at 15 Myr and 25 Myr of two models with prescribed inflow, since 0 Myr, from the SE (M600.SE) and SW (M600.SW) compared with the reference model M600.O*. These models are made with a slightly higher value of $E_{\text{dis}} = 433$ KJ/mol to suppress some small-scale dripping we observed in the plate decoupling zones (Fig. 5; 25 Myr). We also used for these two models a free-slip bottom condition. Both models demonstrate significant differences in shape and slab position with the reference model after 15 Myr of the modeled subduction evolution and increasingly after 25 Myr. Along an E–W orientation the position of the slab tips for models M600.SE and M600.SW differs with the reference model by 200–220 km to the west and to the east respectively, while the trench position for all three models differs by ~ 20 km. At the depth of 660 km the slab in model M600.SE is located ~ 250 to the north, while in the asthenosphere this is 150 km exemplifying the strong lateral bending of the slab. For model M600.SW these differences are somewhat larger amounting to 300 km northward shift in the position of the slab tip. Experiments with a no-slip condition on the bottom lead, as compared to a free-slip bottom (Fig. 7), to a similar slab shape but to ~ 30 km less northward transport of the slab. Overall, these models with imposed oblique mantle flow show the largest differences in the slab shape and position among all conducted experiments and demonstrate a larger sensitivity of slab morphology evolution than observed in the experiments with pure trench-perpendicular or trench-parallel mantle inflow. In these latter experiments the non-obliqueness of the flow direction compared to the overall trench and slab geometry apparently has a stabilizing effect on out-of-slab-plane deformation. In case of trench-perpendicular inflow, the flow is by large equally deflected by the slab in directions south and north and down-dip. For an initially long slab the trench-parallel inflow mostly led to viscous flow coupling with the slab equally at its back- and top-side leading to lateral slab shortening

and lateral transport (Fig. 4). Only when an initially short slab is exposed to trench-lateral flow we observed stronger slab deformation.

We used the M600.O-model setup also for a brief excursion into testing if using open versus closed (free slip) boundaries would lead to a significant difference in modeling results. In model M600.FS we prescribe free-slip conditions on the northern and southern boundary while the west and east boundary remain open for mass balancing of the inflow of the subducting plate. The results, discussed in supplementary materials 1, show that the free-slip boundary condition leads primarily to ~ 50 km less rollback in 25 Myr compared to M600.O. This is likely tied in with differences in the toroidal flow we observe around the slab edge revealing a complex 3D internal flow, which is different for both boundary conditions.

We have also tested free-slip conditions with model M600.FS–W for which free-slip boundary conditions on the western boundary were prescribed while all other boundaries were open. After 25 Myr the observed difference with reference M600.O model was of the order of ~ 10 km, which is even smaller than in the case of M600.FS model. The differences between using open boundaries or partly closed boundaries are much smaller than observed in 2-D subduction modeling (Chertova et al., 2012), which suggests that these differences may diminish in 3D modeling if the boundaries are placed at a large distance.

4. Influence of external mantle flow on the evolution of the RGB and Kabyldes slabs

Departing from the relatively “rectangular” plate configurations in previous experiments, here we advance on an earlier developed 3-D subduction model of western Mediterranean subduction leading to the Rif–Gibraltar–Betics (RGB) slab and the Kabyldes slab in which we used open side boundaries (Chertova et al., 2014a, 2014b). The slab evolution of the RGB slab involves trench rollback in which the trench rotates by more than 180 degrees and where the trench is generally highly oblique to the subduct-

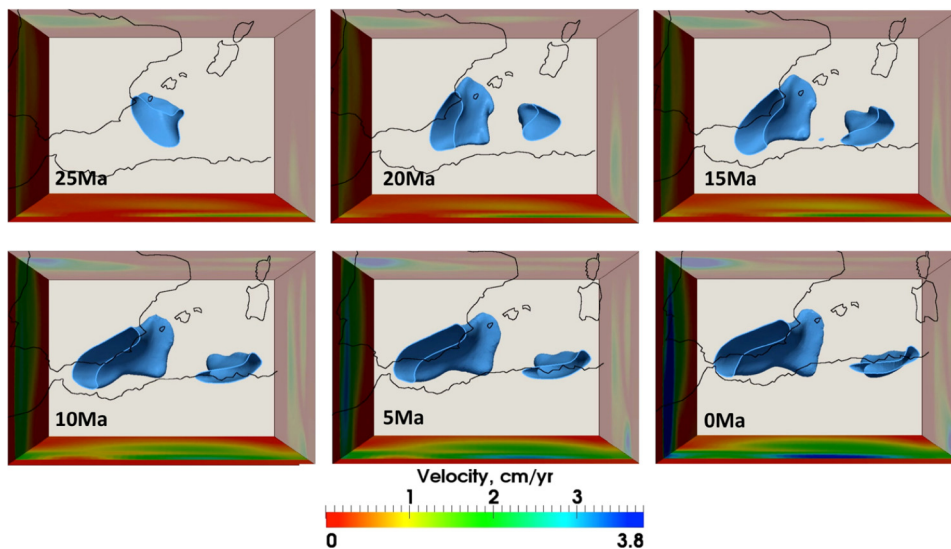


Fig. 8. Model WMED.SW: Evolution of the western Mediterranean subduction under the influence of mantle in/outflow through the southern and western sidewalls. In color the total amplitude of the imposed boundary velocity field is shown. In/Outflow vector are shown in supplementary video 1. In transparent colors we plotted the resulting in/outflow through the open northern and eastern boundaries. The 1400 K isotherm delineates the slabs from 200 km depth downward. The initial, 35–25 Ma, stage is skipped, as both slabs are shallower than 200 km.

ing plate motion. The evolution of this reference subduction model, WMED.O, are described in detail in the supplementary material 1.

The prescribed time-dependent mantle flow is determined from back-advection of a density and temperature model derived from the global tomographic model P06_CSloc (Amaru, 2007) and surface plate velocities (Torsvik et al., 2010), and expanded to spherical harmonic degree 63. We convert seismic velocity anomalies to density anomalies, first assuming they are both due to temperature anomalies and hence using a thermal conversion factor shown in supplementary Fig. 7. However, we remove any strong positive anomalies in the continental lithosphere, which are most likely not due to temperature anomalies, with a procedure described in Steinberger et al. (2015). Mantle flow is computed with an extension of the method of Hager and O'Connell (1981) that accounts for compressibility, depth-dependent gravity and phase boundaries, with a suitable radial viscosity structure shown in supplementary Fig. 1. Based on this flow field we use downwind differencing to compute derivatives of density with respect to time at grid points. Time integration is done with a fourth-order Runge–Kutta scheme. Other details of the computation are explained in the supporting information of Steinberger et al. (2015). We also compared the predicted mantle flow from model P06_CSloc with that predicted from three other tomographic models and found general agreement on the style, in- or outflow, and good agreement in the average amplitude for all boundaries (supplementary Fig. 8).

The mantle flow prescribed on 4 side boundaries is shown in supplementary movie 1. Although this model features the tomographic image of the RGB slab, the locally predicted flow may still not be consistent with the numerically modeled slab for which a no-slip condition at the bottom of the model is used. Imposing flow at all boundaries combined with net inflow of the lithosphere plates violates mass balance. Proper attention for conservation of the model mass balance is required and therefore we impose the calculated flow at only two adjacent sides per experiment, treating the other two sides as open boundaries.

We first test effects of mantle in/outflow at the northern and eastern sides of the model and next at the southern and western parts. Fig. 8 shows the evolution of both slabs when mantle in/outflow is prescribed on the southern and western boundaries (model WMED.SW). The amplitude of the prescribed mantle in/outflow is shown in color on the domain boundaries. Mantle in- and outflow

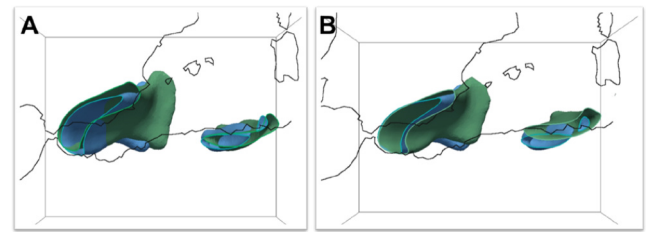


Fig. 9. A. Comparison after 35 Myr of subduction evolution between the reference model WMED.O (blue) and model WMED.SW (green) with prescribed in/outflow on the southern and western sidewalls. B. Comparison after 35 Myr of subduction evolution between the reference model WMED.O (blue) and model WMED.NE (green) with prescribed in/outflow on the northern and eastern sidewalls. The 1400 K isotherm delineating the slabs is shown from 200 km depth downward.

is also shown in the supplementary movie 1. The subduction of both slabs evolves in a similar way as in model WMED.O (supplementary Fig. 5) and in both models the RGB and Kabylides slabs reach their present-day position after 35 Myr of slab evolution, while the overall shape of the slabs is similar (Fig. 9A). In model WMED.SW the amount of lithosphere tearing for the RGB slab along the east Iberian margin since ~10 Ma is smaller than in the reference model. This effect correlates with the strong inflow at the western boundary since 10 Ma. This mantle flow supports the slab from below and counteracts the downward slab pull leading to reduced tearing of the Iberian margin. The external flow also leads to a slightly more easterly position of the deep slab and a slight shallowing in overall slab tilt (Fig. 9A). This effect is similar to that observed in our earlier generic models where westward slab rollback was counteracted by opposite mantle inflow in the sub-slab region (e.g. model M600.W; Fig. 5).

In Fig. 9B we show the comparison with model WMED.NE, which is based on predicted in/outflow from the north and east, with the reference model WMED.O at the final stage reached after 35 Myr of model evolution. Also, here the overall position and shape of the slabs are similar, while lithosphere tearing under the Iberian margin has also started to develop in model WMED.NE. Also now a change in slab tilt is observed although somewhat smaller than in model WMED.SW. The Kabylides slab is located more to the north, which is in better agreement with its tomographic image (Chertova et al., 2014a, 2014b).

The differences between WMED.SW, WMED.NE, and the reference model WMED.O are generally of the order of 10–50 km, which is small compared to the overall distance traveled by slab rollback and to the overall match in slab position and morphology. The difference in eastward slab tilt leads to an eastward shift of the slab geometry in the transition zone of ~ 100 km. Important for our previous work (Chertova et al., 2014a, 2014b) is that this demonstrates the robustness of the overall slab position and geometry of the RGB and Kabyldes slabs obtained after 35 Myr of modeled subduction evolution with respect to the influence of external mantle flow.

5. Discussion and conclusions

Using 3D numerical thermo-mechanical modeling within a regional model domain we investigated the influence of remotely forced mantle flow on subduction and slab morphology evolution. The nonlinear composite rheology we used is adopted from Chertova et al. (2014a, 2014b) and conforms to the present-day knowledge of mantle rheology (e.g. King, 2016). Experiments were performed for both a generic setup similar to that used by others and for a natural example in the western Mediterranean with a complex spatial-temporal slab evolution. Within each geometric setting similar effects of external mantle flow on subduction evolution could be observed which mostly concerned various morphological changes on the scale of 10–50 km and appreciable differences in total rollback of order of 50 km, all accumulating in 25 Myr of modeled subduction, or 35 Myr for the western Mediterranean subduction systems.

Mantle flow perpendicular to the trench, from either direction, proved the least influential on internal slab deformation, apart from slight changes in slab dip, which can be explained by the fact that such flow is deflected trench-parallel to both sides and thus affects the slab equally along its width. We observed no strong (e.g. tens of degrees) change in the dip of the narrow or wide slab resulting from trench-perpendicular mantle flow. This is in contrast with observations from 2-D subduction modeling with an imposed horizontal mantle flow of similar amplitude (3 cm/yr) used for investigating the effects on slab dip of a proposed eastward directed global mantle flow (Rodríguez-González et al., 2014; Ficini et al., 2017). In our 3-D experiments, slab lateral mantle flow and toroidal mantle flow around provide lateral transport of mantle material at either side of the slab without strongly affecting the slab dip.

Trench-parallel inflow led to large ~ 150 km trench-parallel transport of the slab, which in our models is taken up in the weak plate-coupling zones at either side of the subducting and in lateral deformation of the side plates. On Earth this lithosphere motion is likely more restricted which suggests instead an amplification of the slab bending and thickening effects we observed in the various experiments in response to the viscous coupling with slab-parallel or obliquely impacting flow. In reality slab deformation due to trench-parallel flow may also impact on the crustal evolution in the overlying crust potentially leading to trench-parallel shortening or stretching above slab edges.

We also observed that narrow (660 km) slabs are comparably affected as wide (1400 km) slabs, which is an expression of the fact that the total frictional force acting on the slab scales with its surface area while the detail of slab morphology change is caused by viscous tractions of similar amplitude. Long slabs that reached the transition zone before the onset of trench-parallel flow experience less morphology change, although they are still transported over 150 km or more. Various experiments with mantle flow impacting obliquely on the slab surface proved to have much larger impact on slab deformation giving rise to strong out-of-plane slab bending of more than 200 km and changes in overall slab tilt.

In our last experiments concerning simulations of natural subduction in the western Mediterranean during the past 35 Myr, we imposed past mantle flow determined from a tomographic model of present-day mantle structure. Apart from the complexities and uncertainties that are entailed in determining this past flow, we observed for the predicted spatially and temporally varying mantle flow that the overall position and slab morphology of the RGB and Kabyldes slabs are rather robust with respect to 35 Myr of external flow impact on subduction evolution. The differences between the three simulations concern slab tilt and morphological changes of the scale of 10–50 km, which is still an important scale to be considered for orogenic geological processes in the overlying crust.

All our experiments suggest that during a long period of subduction the slab forcing by external mantle flow is of secondary importance with respect to the forcing by slab buoyancy and imposed plate motions that control the first-order aspects of long-term subduction evolution. However, we have shown that various aspects of slab morphology (e.g. slab bending, slab edge thickening, slab tilt) and subduction evolution (e.g. rollback speed and trench deformation) can result from the continuous impact of remotely forced mantle flow. At present these aspects may be difficult to discern from other processes that determine slab morphology, e.g. subduction of trench-parallel lithosphere heterogeneity (e.g. Moresi et al., 2014; Duretz et al., 2014) or other complexity of the geodynamic subduction setting (e.g. Boutelier and Cruden, 2013; Chertova et al., 2014a, 2014b). An additional complexity is that the still large uncertainty in mantle rheology allows for trade-offs in numerical modeling between variations in mantle flow and mantle rheology. Still the contribution to slab deformation from long-term impact of remotely excited mantle flow cannot be ignored when considering the crustal evolution overhead. To make steps forward, deciphering the various contributions requires more detailed numerical modeling that includes the crustal response as well as independent observations from geology, geodesy, and geophysics, for instance by higher-resolution seismic tomography models and by spatially dense observations of seismic anisotropy.

Acknowledgements

We thank Hana Čížková for helpful comments on the original manuscript. M.V.C. and W.S. acknowledge financial and computational support from ISES, the Netherlands research centre for Integrated Solid Earth Science. W.S. and B.S. also acknowledge support from the Research Council of Norway through its Centres of Excellence funding scheme, project number 223272.

Appendix A. Supplementary material

Supplementary material related to this article can be found online at <https://doi.org/10.1016/j.epsl.2018.02.038>.

References

- Amaru, M.L., 2007. Global Travel Time Tomography with 3-D Reference Models. PhD Thesis. Utrecht University.
- Boutelier, D.A., Cruden, A.R., 2008. Impact of regional mantle flow on subducting plate geometry and interplate stress: insights from physical modeling. *Geophys. J. Int.* 174 (2), 719–732. <https://doi.org/10.1111/j.1365-246X.2008.03826.x>.
- Boutelier, D., Cruden, A., 2013. Slab rollback rate and trench curvature controlled by arc deformation. *Geology* 41 (8), 911–914. <https://doi.org/10.1130/G34338.1>.
- Butterworth, N.P., Quevedo, L., Morra, G., Müller, R.D., 2012. Influence of overriding plate geometry and rheology on subduction. *Geochem. Geophys. Geosyst.* 13 (6). <https://doi.org/10.1029/2011GC003968>.
- Capitanio, F.A., Faccenda, C., 2012. Complex mantle flow around heterogeneous subducting oceanic plates. *Earth Planet. Sci. Lett.* 353–354, 29–37. <https://doi.org/10.1016/j.epsl.2012.07.042>.

- Capitanio, F.A., Stegman, D.R., Moresi, L.N., Sharples, W., 2010. Upper plate controls on deep subduction, trench migrations and deformations at convergent margins. *Tectonophysics* 483, 80–92. <https://doi.org/10.1016/j.epsl.2012.07.042>.
- Chertova, M., Geenen, T., van den Berg, A.P., Spakman, W., 2012. Using open sidewalls for modeling self-consistent lithosphere subduction dynamics. *Solid Earth* 3, 313–326. <https://doi.org/10.5194/se-3-313-2012>.
- Chertova, M.V., Spakman, W., Geenen, T., van den Berg, A.P., van Hinsbergen, D.J.J., 2014a. Underpinning tectonic reconstructions of the western Mediterranean region with dynamic slab evolution from 3-D numerical modeling. *J. Geophys. Res.*, *Solid Earth* 119 (7), 5876–5902. <https://doi.org/10.1002/2014JB011150>.
- Chertova, M.V., Spakman, W., van den Berg, A.P., van Hinsbergen, D.J.J., 2014b. Absolute plate motions and regional subduction evolution. *Geochim. Geophys. Geosyst.* 15 (10), 3780–3792. <https://doi.org/10.1002/2014GC005494>.
- Cramer, F., Tackley, P.J., 2014. Spontaneous development of arcuate single-sided subduction in global 3-D mantle convection models with a free surface. *J. Geophys. Res.*, *Solid Earth* 119. <https://doi.org/10.1002/2014JB010939>.
- Dobrovine, P.V., Steinberger, B., Torsvik, T.H., 2012. Absolute plate motions in a reference frame defined by moving hotspots in the Pacific, Atlantic and Indian oceans. *J. Geophys. Res.* 117, B09101. <https://doi.org/10.1029/2011JB009072>.
- Duretz, T., Gerya, T.V., Spakman, W., 2014. Slab detachment in laterally varying subduction zones: 3-D numerical modeling. *Geophys. Res. Lett.* 41 (6), 1951–1956. <https://doi.org/10.1002/2014GL059472>.
- Ficini, E., Dal Zilio, L., Doglioni, C., Gerya, T.V., 2017. Horizontal mantle flow controls subduction dynamics. *Sci. Rep.* 7, 7550. <https://doi.org/10.1038/s41598-017-06551-y>.
- Funiciello, F., Faccenna, C., Giardini, D., Regenauer-Lieb, K., 2003. Dynamics of retreating slabs: insights from three-dimensional laboratory experiments. *J. Geophys. Res.* 108 (B4), 2207. <https://doi.org/10.1029/2001JB000896>.
- Funiciello, F., Faccenna, C., Giardini, D., 2004. Role of lateral mantle flow in the evolution of subduction systems: insights from laboratory experiments. *Geophys. J. Int.* 157, 1393–1406. <https://doi.org/10.1111/j.1365-246X.2004.02313.x>.
- Funiciello, F., Moroni, M., Piromallo, C., Faccenna, C., Cenedese, A., Bui, H.A., 2006. Mapping mantle flow during retreating subduction: laboratory models analyzed by feature tracking. *J. Geophys. Res.* 111. <https://doi.org/10.1029/2005JB003792>.
- Guillaume, B., Husson, L., Funiciello, F., Faccenna, C., 2013. The dynamics of laterally variable subductions: laboratory models applied to the Hellenides. *Solid Earth Discuss.* 5 (1), 315–363. <https://doi.org/10.5194/se-4-179-2013>.
- Hager, B.H., O'Connell, R.J., 1981. A simple global model of plate dynamics and mantle convection. *J. Geophys. Res.* 86, 4843–4867.
- Hager, B.H., O'Connell, R.J., Raefsky, A., 1983. Subduction, back-arc spreading and global mantle flow. *Tectonophysics* 99, 165–189.
- Heuret, A., Lallemand, S., 2005. Plate motions, slab dynamics and back-arc deformation. *Phys. Earth Planet. Inter.* 149, 31–51. <https://doi.org/10.1016/j.pepi.2004.08.022>.
- Jadamec, M.A., Billen, M.I., 2012. The role of rheology and slab shape on rapid mantle flow: three-dimensional numerical models of the Alaska slab edge. *J. Geophys. Res.* 117, B02304. <https://doi.org/10.1029/2011JB008563>.
- Kincaid, C., Griffiths, R.W., 2003. Laboratory models of the thermal evolution of the mantle during rollback subduction. *Nature* 425, 58–62. <https://doi.org/10.1038/nature01923>.
- King, S.D., 2016. Reconciling laboratory and observational models of mantle rheology in geodynamic modeling. *J. Geodyn.* 100, 33–50. <https://doi.org/10.1016/j.jog.2016.03.005>.
- MacDougall, J.G., Kincaid, C., Szwaja, S., Fischer, K.M., 2014. The impact of slab dip variations, gaps and rollback on mantle wedge flow: insights from fluids experiments. *Geophys. J. Int.* 197, 705–730. <https://doi.org/10.1093/gji/ggu053>.
- Meyer, C., Schellart, W.P., 2013. Three-dimensional dynamic models of subducting plate-overriding plate-upper mantle interaction. *J. Geophys. Res.*, *Solid Earth* 118, 775–790. <https://doi.org/10.1002/jgrb.50078>.
- Moresi, L., Betts, P.G., Miller, M.S., Cayley, R.A., 2014. Dynamics of continental accretion. *Nature* 508, 245–248. <https://doi.org/10.1038/nature13033>.
- Olbertz, D., Wortel, M.J.R., Hansen, U., 1997. Trench migration and subduction zone geometry. *Geophys. Res. Lett.* 240, 221–224.
- Piromallo, C., Becker, T.W., Funiciello, F., Faccenna, C., 2006. Three-dimensional instantaneous mantle flow induced by subduction. *Geophys. Res. Lett.* 33, L08304. <https://doi.org/10.1029/2005GL025390>.
- Rodríguez-González, J., Negredo, A.M., Carminati, E., 2014. Slab-mantle flow interaction: influence on subduction dynamics and duration. *Terra Nova* 26, 265–272. <https://doi.org/10.1111/ter.12095>.
- Schellart, W.P., 2004. Kinematics of subduction and subduction-induced flow in the upper mantle. *J. Geophys. Res.* 109, B07401. <https://doi.org/10.1029/2004JB002970>.
- Schellart, W.P., 2008. Overriding plate shortening and extension above subduction zones: a parametric study to explain formation of the Andes Mountains. *Geol. Soc. Am. Bull.* 120 (11–12), 1141–1454. <https://doi.org/10.1130/B26360.1>.
- Schellart, W.P., Moresi, L., 2013. A new driving mechanism for backarc extension and backarc shortening through slab sinking induced toroidal and poloidal mantle flow: results from dynamic subduction models with an overriding plate. *J. Geophys. Res.*, *Solid Earth* 118, 3221–3248. <https://doi.org/10.1002/jgrb.50173>.
- Schellart, W.P., Freeman, J., Stegman, D.R., Moresi, L., May, D., 2007. Evolution and diversity of subduction zones controlled by slab width. *Nature Lett.* 446. <https://doi.org/10.1038/nature05615>.
- Segal, A., Praagman, N., 2005. The Sepran FEM Package. Technical Report. Ingenieursbureau Sepra, The Netherlands. <http://ta.twi.tudelft.nl/sepran/sepran.html>.
- Stegman, D.R., Farrington, R., Capitanio, F.A., Schellart, W.P., 2010. A regime diagram for subduction styles from 3-D numerical models of free subduction. *Tectonophysics* 483, 29–45. <https://doi.org/10.1016/j.tecto.2009.08.041>.
- Stegman, D.R., Freeman, J.J., Schellart, W.P., Moresi, L., May, D., 2006. Influence of trench width on subduction hinge retreat rates in 3-D models of slab rollback. *Geochim. Geophys. Geosyst.* 7, 1–22. <https://doi.org/10.1029/2005GC001056>.
- Steinberger, B., Spakman, W., Japsen, P., Torsvik, T.H., 2015. The key role of global solid Earth processes in the late Cenozoic intensification of Greenland glaciation. *Terra Nova* 27, 1–8. <https://doi.org/10.1111/ter.12133>.
- Sternai, P., Jolivet, L., Menant, A., Gerya, T., 2014. Driving the upper plate surface deformation by slab rollback and mantle flow. *Earth Planet. Sci. Lett.* 305, 110–118. <https://doi.org/10.1016/j.epsl.2014.08.023>.
- Torsvik, T.H., Steinberger, B., Gurnis, M., Gaina, C., 2010. Plate tectonics and net lithosphere rotation over the past 150 Myr. *Earth Planet. Sci. Lett.* 291, 106–112. <https://doi.org/10.1016/j.epsl.2009.12.055>.
- van Hinsbergen, D.J.J., Vissers, R.L.M., Spakman, W., 2014. Origin and consequences of western Mediterranean subduction, rollback, and slab segmentation. *Tectonics* 33. <https://doi.org/10.1002/tect.20125>.
- Winder, R.O., Peacock, S.M., 2001. Viscous forces acting on subducting lithosphere. *J. Geophys. Res.* 106 (21), 21937–21951.
- Yamato, P., Husson, L., Braun, J., Loiselet, C., Thieulot, C., 2009. Influence of surrounding plates on 3D subduction dynamics. *Geophys. Res. Lett.* 36, L07303. <https://doi.org/10.1029/2008GL036942>.